Photosynthesis Research (2005) 85: 73–86

Review

X-ray spectroscopy of the Mn_4Ca cluster in the water-oxidation complex of Photosystem II

Kenneth Sauer[1,2,*], Junko Yano[1,2,*] & Vittal K. Yachandra[2,*]
[1]*Department of Chemistry, University of California, Berkeley, CA 94720-1460, USA;* [2]*Melvin Calvin Laboratory, Physical Biosciences Division, Lawrence Berkeley National Laboratory, Berkeley, CA 94720, USA; *Authors for correspondence (e-mail: khsauer@lbl.gov; jyano@lbl.gov; vkyachandra@lbl.gov; fax: +1-510-486-6059)*

Received 3 November 2004; accepted in revised form 13 January 2005

Key words: EXAFS, manganese cluster, oxygen evolution, Photosystem II, water-oxidation, X-ray dichroism, X-ray spectroscopy

Abstract

The water-oxidation complex of Photosystem II (PS II) contains a heteronuclear cluster of 4 Mn atoms and a Ca atom. Ligands to the metal cluster involve bridging O atoms, and O and N atoms from amino acid side-chains of the D1 polypeptide of PS II, with likely additional contributions from water and CP43. Although moderate resolution X-ray diffraction-based structures of PS II have been reported recently, and the location of the Mn_4Ca cluster has been identified, the structures are not resolved at the atomic level. X-ray absorption (XAS), emission (XES), resonant inelastic X-ray scattering (RIXS) and extended X-ray absorption fine structure (EXAFS) provide independent and potentially highly accurate sources of structural and oxidation-state information. When combined with polarized X-ray studies of oriented membranes or single-crystals of PS II, a more detailed picture of the cluster and its disposition in PS II is obtained.

Abbreviations: EPR – electron paramagnetic resonance; EXAFS – extended X-ray absorption fine structure; PS II – Photosystem II; RIXS – resonant inelastic X-ray scattering; XANES – X-ray absorption near-edge structure; XAS – X-ray absorption spectroscopy; XES – X-ray emission spectroscopy

Introduction

Photosystem II contains the oxygen evolving complex that is responsible for the presence of the oxygen in Earth's atmosphere. This complex contains a cluster of 4 Mn and a Ca, and O_2 evolution activity is enhanced by Cl (Olesen and Andréasson 2003) that may also be present in the cluster (Yachandra et al. 1996). The ability to produce oxygen photosynthetically is shared by eukaryotic plants and algae and by prokaryotic cyanobacteria. Geologic evidence indicates that cyanobacteria were present 3.5 Ga (3.5 billion years) ago (Schopf 1999). Investigations in plants, algae and cyanobacteria indicate that the water-oxidation complexes, as they exist today, are almost indistinguishable in structure and activity, despite having diverged more than a billion years ago.

Many photosynthetic bacteria and archae use powerful reducing agents like hydrogen, hydrogen sulfide or a variety or organic reductants to supply their metabolic energy (Blankenship et al. 1995). Most of these organisms do not tolerate oxygen, or they change in its presence to a non-photosynthetic manifestation to continue to grow. The challenge from using water as a reducing agent in the light reactions associated with photosynthesis is that it is a poor reductant and requires a high

electrochemical potential to produce dioxygen as a product. The high potential is produced by the photo-induced product of electron transfer from the reaction center, P_{680}, in PS II (Blankenship 2002). The removed electrons are passed to a pair of plastoquinone molecules that, in turn, transmit them by an electron transport chain to Photosystem I, where an additional light reaction produces the low-potential electrons and reductants that are involved in CO_2 reduction chemistry of the Calvin cycle. This two-light reaction scheme is exclusive to higher plants, algae and cyanobacteria, where water is the reductant. Non-oxygen evolving photosynthetic bacteria use a single light reaction to drive the redox reactions associated with the more powerfully reducing chemical substrates (Blankenship et al. 1995).

The photo-oxidation product, P_{680}^{+}, proceeds to extract electrons from associated membrane-bound donors – first a tyrosine, Y_Z, and then from the Mn cluster. An important function of this cluster is to retain oxidizing equivalents from single-electron transfer light reactions to facilitate the 4-electron transfer process that is responsible for the formation of one O_2 molecule from two water molecules:

$$2H_2O \rightarrow O_2 + 4H^+ + 4e^-$$

Since it was first realized that Mn is an essential element for photosynthetic water oxidation, investigators have sought ways to determine the features of its structural environment and the details of its involvement. A variety of spectroscopic methods have been employed, among them, the most valuable being electron paramagnetic resonance (EPR) and X-ray spectroscopy (Powers 1982; Yachandra 1995; Yachandra et al. 1996; Penner-Hahn 1998; Yachandra 2002; Britt et al. 2004). Each of these approaches comes in a variety of forms. The spectroscopic studies have been greatly aided by studies of site-specific mutants, particularly in the D1 protein of PS II, which provides ligands to the metal cluster (Debus 2001), and by the recent publications of structural models of PS II based on X-ray diffraction (Zouni et al. 2001; Kamiya and Shen 2003; Biesiadka et al. 2004; Ferreira et al. 2004). These structures, while limited by resolution currently in the 3.2–3.5 Å range and falling short of atomic resolution, nevertheless serve to locate the electron density associated with the Mn and Ca in the multi-protein PS II complex and to confirm the ligand candidates that are available in the vicinity. Unfortunately, using the high X-ray radiation dosage necessary to accumulate data for the X-ray diffraction analysis, the Mn in the cluster is highly susceptible to reduction by Mn^{2+} (J. Yano et al., in preparation). Inevitably, the local bonding that determines the cluster geometry is destroyed at the same time. Fortunately, highly precise structural information can be obtained by X-ray spectroscopic methods that do not involve such high radiation doses and, in fact, provide a clear indicator when such radiation damage does occur.

X-ray spectroscopic studies of Photosystem II

X-ray spectroscopy is similar to UV-visible spectroscopy, except that typical K-edge X-ray energies of metals pertinent to the Mn_4Ca cluster exceed 4000 eV, whereas the normal UV–visible region is in the 1.5–4 eV range. Transitions involving core electrons are involved in absorption or emission of X-rays, and the transition energies are highly element specific. For example, the K-edge X-ray absorption near-edge structure (XANES) associated with the excitation of an electron from the 1s orbital of Mn to a bound 3d or unoccupied 4p orbital (or LUMO) requires energies of ~6500 eV (Figure 1a). For elements adjacent to Mn in the Periodic Table, the K-edge energies occur at ~5450 eV for Cr and at ~7100 eV for Fe. Thus, there is a region of the spectrum in which the transitions of Mn are dominant. The exact energies at which specific transitions for a particular element occur are dependent, in part, on its oxidation state and its coordination environment. This dependence can provide both chemical and structural information from a detailed examination of the XANES region (Yachandra 1995). Information about metal–atom oxidation-state changes that is less influenced by the nature of coordinating ligands is obtained from XES. For metals in the first transition series, Kβ emission results from X-ray absorption at an energy somewhat above the K-edge followed by an emissive transition that transfers an electron from a metal 3p to 1s orbital, as illustrated in Figure 1b (Bergmann et al. 1998). This approach has the advantage that transitions involving 3p electrons rather than 4p orbitals are involved; the former are

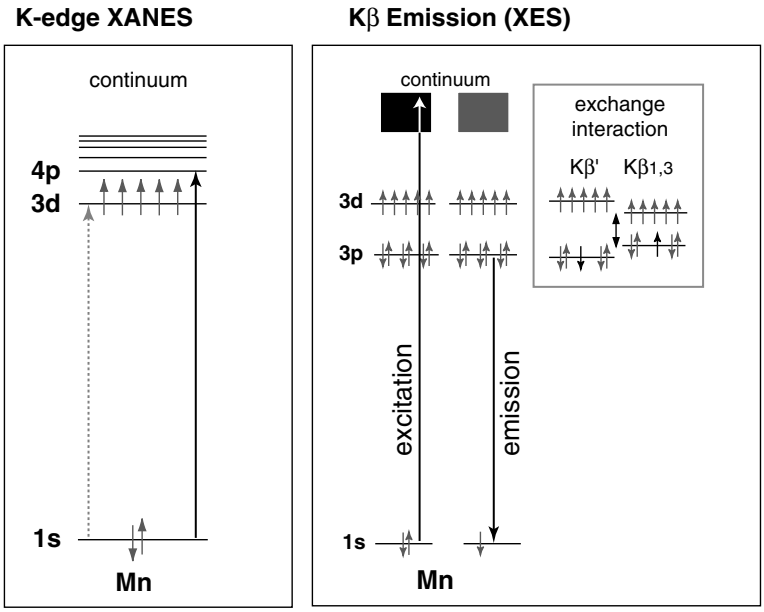

Figure 1. Energy level diagrams showing the origin of Kα X-ray absorption near-edge structure (XANES) and Kβ X-ray emission spectra (XES) for elements in the first transition-metal series. Exchange interaction with ligand orbitals leads to a splitting of the Kβ transition, as seen in Figure 4.

less likely to be influenced by mixing with ligand orbitals that may be perturbed by small differences in the metal coordination.

At energies somewhat greater, the absorption of an X-ray provides sufficient energy to cause the absorbing atom to release the electron (ionize). Any excess energy is carried off as translational kinetic energy, which is alternatively reflected in the wavelength associated with the electron treated as a wave phenomenon. In condensed phase, such as a metalloprotein, the released electron scatters off nearby atoms, resulting in an interference pattern in the absorption intensity in this X-ray energy region above the absorption edge. The interference pattern can be transformed (Fourier-transformed) into a distance-dependent profile centered on the emitting atom. This profile is known as extended X-ray absorption fine structure (EXAFS) and contains highly useful information about bond distances of coordinating atoms out to about ~5 Å from the absorbing atom. The general nature of the scattering atom can often be deduced from the fact that scattering intensity increases with the electron density (i.e., atomic number) of the scattering atom (Powers 1982; Yachandra 1995). An additional consequence of these released electrons is the incidence of radiation damage. The interaction of the high energy electrons with the matrix induces the formation of free radicals and further chemical reactions that degrade the molecules. In the case of metallo-proteins, a common consequence is chemical reduction of the metal centers. As we have observed directly, Mn in the water oxidation complex of PS II is particularly sensitive to this kind of radiation damage, which is seen in terms of its reduction and conversion to Mn^{2+} following exposure to even modest doses of X-ray radiation.

Using oriented samples, and polarized X-rays, emitted at high intensities from the synchrotron sources of X-rays used for spectroscopy, information about the relative directions of the scattering atoms is also available. In the photosynthetic studies, both one-dimensional ordered membrane preparations and three-dimensional single-crystal studies of PS II have been carried out.

Some of the first X-ray spectroscopy on metal centers in any biological material was carried out on photosynthetic materials. Earlier X-ray spectroscopy was dominated by studies of pure samples of simple molecules. Metallo-enzymes presented a challenge because of the small relative

concentration of the element of interest. In photosynthetic materials, the Mn may be at the level of 10 parts per million or less. A breakthrough in technology that enabled such materials to be investigated with good sensitivity was achieved by our colleague Mel Klein at the Lawrence Berkeley National Laboratory and collaborators. The use of X-ray induced fluorescence to investigate these samples yields signals that are much less contaminated by interfering background (Jaklevic et al. 1977). This is the standard approach now used by essentially all X-ray spectroscopists who deal with these materials. Subsequent improvements in X-ray monochromators, in detector and cryostat technology, together with the advance of a theoretical basis for analyzing the spectra, have steadily improved the quality of the data and their interpretation.

The requirements of X-ray spectroscopy place some restrictions with respect to sample preparation and experimental conditions. The investigation of light elements can present difficulties because of the presence of an aqueous medium and because of the pervasive occurrence of C, N and O in biological materials. In X-ray energy regions where atmospheric gases absorb, samples must be placed in an atmosphere of helium or in vacuum. In our studies, we have succeeded in measuring X-ray spectra for transition elements like Mn, Fe and Mo, as well as for Ca, Sr, S, Se, Cl and Br. For elements like Ca and Cl, which can occur in a wide variety of environments in biological materials, it is particularly challenging to remove sources of background signals that greatly complicate the interpretation of the results. Making measurements at low temperature such as 100 K or even lower at 10 K, significantly decreases the extent of radiation damage and improves resolution. Sensitivity is improved by concentrating the samples, often to the point of making a viscous paste; even better quality spectra are achieved through the use of crystalline samples. Nevertheless, quite small sample sizes are often sufficient – in the order of 1 μl or less using focused beams from synchrotron sources. All of these approaches have proved valuable in the case of PS II.

The first published X-ray absorption spectrum of a leaf showed a pronounced peak attributable to Mn (Jaklevic et al. 1977). Although it was not commented at the time, the signal undoubtedly was dominated by aqueous or other non-specific Mn^{2+} present in the leaf. In subsequent studies, samples enriched in PS II and washed free of unbound or loosely bound Mn^{2+} were used. The landmark studies of this nature were carried out on broken chloroplasts and were published by the Klein group in a pair of papers in 1981. Part 1 presented an analysis of the EXAFS of Mn, concluding that the spectra showed evidence of the presence of di-μ-oxo bridged pairs of Mn atoms in the PS II cluster (Kirby et al. 1982a). As in all studies of this nature, the results were interpreted using insights gained from the study of a variety of model complexes whose precise structures are known from X-ray diffraction. Inactivation of the PS II samples leading to release of Mn resulted in substantial alteration of the EXAFS spectra. Part 2 described an analysis of the X-ray absorption edges (Kirby et al. 1982b). Even in these first studies, it could be readily seen that inactivation of the chloroplasts also produced a shift in the edge energy that is characteristic of Mn reduction. The next publication reported that illumination of PS II samples in the S_1-state causes a shift of the Mn X-ray absorption edge to higher energies, characteristic of Mn oxidation from S_1 to S_2 state (Goodin et al. 1984). In this first group of papers, the usefulness of X-ray absorption-edge studies in relating to Mn oxidation-state changes was established.

Using techniques involving stabilization at low temperature, individual S-states could be produced and investigated by XAS (Yachandra et al. 1986a, b). Clear differences in absorption edge energy attributed to Mn oxidation were seen in the $S_0 \rightarrow S_1$ and $S_1 \rightarrow S_2$ transitions, but the absorption edges for S_2 and S_3 did not show a significant difference. An updated view of this situation using refined experimental techniques (see below and Messinger et al. (2001)) is illustrated in Figure 2. These results were taken to indicate the absence of Mn oxidation during the $S_2 \rightarrow S_3$ transition. In the same 1986 report (Yachandra et al. 1986b), it was shown that the EXAFS is interpretable as shells at 1.8 and 2.0 Å (peak I) attributable to N or O atoms and a shell at 2.7 Å (peak II) from Mn–Mn interactions. An additional shell from Mn was seen at 3.3 Å (peak III) (Figure 3). These observations were indistinguishable between the S_1 and S_2 states and between higher plants and the thermophilic cyanobacterium *Synechococcus*. This study provided a solid framework for incorporating subsequent enhancements

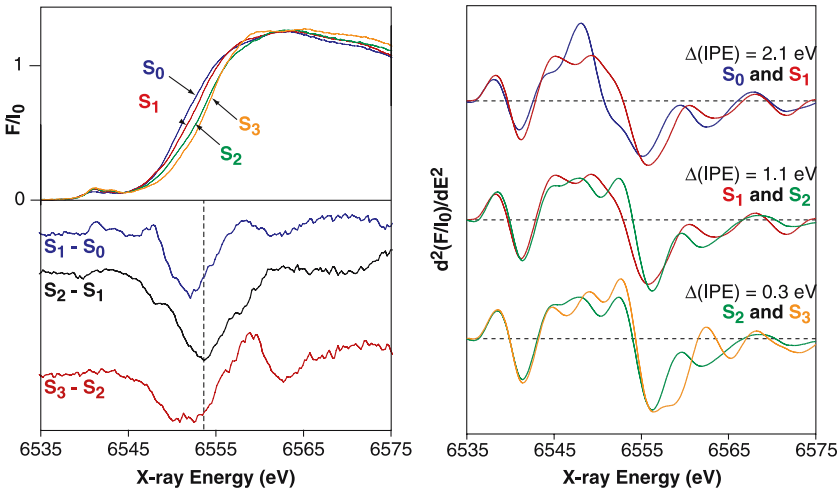

Figure 2. Mn K-edge XANES spectra of individual S-states obtained by deconvolution of spectra obtained from PS II samples illuminated with single-turnover 9-ns flashes (Left upper frame). (Left lower frame) S-state XANES difference spectra, multiplied by factor 5 and vertically offset for clarity, are shown for adjacent pairs of states. The dashed vertical line is at the inflection point energy for the S_2-state spectrum. (Right frame) These spectra are the second derivatives of the S-state XANES edge spectra shown in the upper-left portion of the figure.

that resulted from refinements in the experimental measurements.

Oxidation states of the Mn_4 cluster

Although there has been a general agreement with respect to the increasing oxidation of Mn in the cluster during $S_0 \rightarrow S_1$ and $S_1 \rightarrow S_2$, several reports expressed disagreement concerning the lack

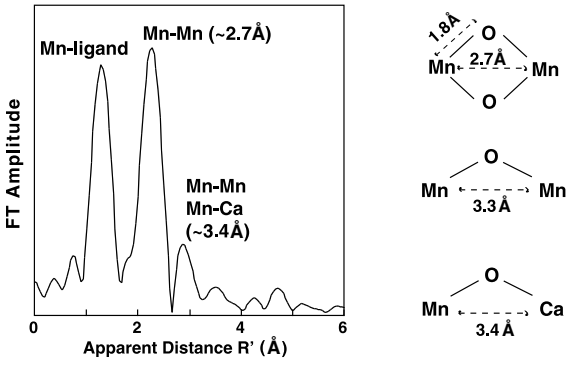

Figure 3. Mn-EXAFS of the S_1-state for a solution of PS II membranes. Composite peak I with components at 1.8 and 2.0 Å is assigned to O and N ligand atoms joined to Mn. Peak II at 2.7 Å results from the contribution of binuclear Mn di-μ-oxo bridged atoms. Peak III at 3.3–3.4 Å has contributions from both Mn–Mn and Mn–Ca interactions. Apparent distances shown on the horizontal axis must be increased owing to a phase factor associated with the Mn scattering atom.

of Mn oxidation during $S_2 \rightarrow S_3$ (Ono et al. 1992; 1995; Iuzzolino et al. 1998). These investigations used saturating flashes to advance the S-states one step at a time, but there is typically significant dephasing owing to double turnovers or complete misses following a flash. The dephasing requires a difficult deconvolution of the resulting spectra to extract the contributions from individual S-states. Roelofs et al. (1996) adopted a more precise procedure for carrying out the deconvolution by using the EPR multi-line signal to determine, for each flashed sample, the amount of the S_2-state present. This approach allowed a more precise determination of the fraction of double hits and misses for each of the same samples whose X-ray spectra were measured. Again, only a small edge-energy difference was seen between S_2 and S_3. Because the controversy persisted and included disagreements on how the edge energy should be measured and characterized, a new approach using very short (9 ns) laser flashes to minimize double hits showed even clearer evidence (Figure 2) to verify the absence of significant oxidation during $S_2 \rightarrow S_3$ (Messinger et al. 2001). In this same study, a new technique using Mn Kβ X-ray emission spectra (XES) was adopted (Figure 4). This approach has the advantage that transitions involving 3p electrons rather than 4p orbitals are involved (see Figure 1); the former are less likely to be influenced

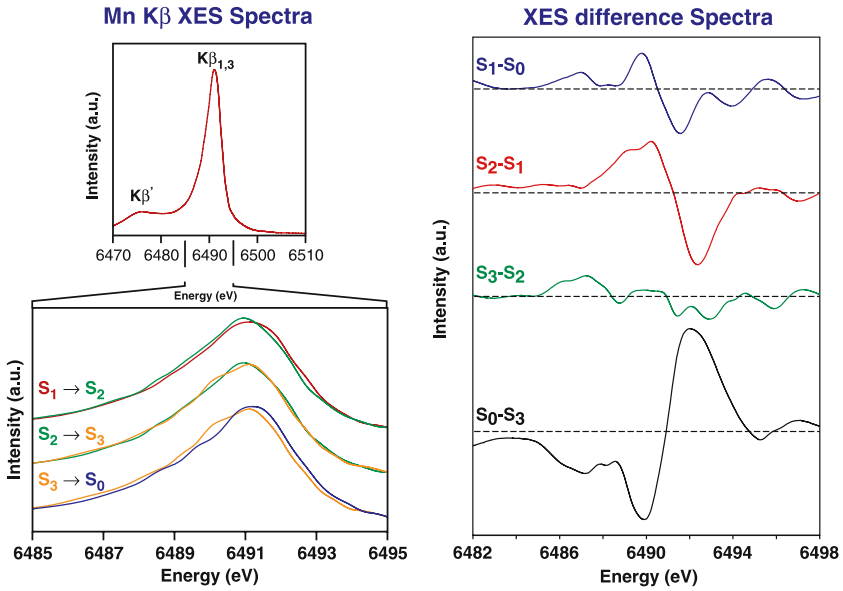

Figure 4. Mn Kβ X-ray emission spectra (XES) of individual S-states produced by the method described in Figure 2. The Mn Kβ XES spectrum (upper left) shows the split emission band mentioned in the Figure 1 caption. Below it are expanded segments showing the $K\beta_{1,3}$ peak for individual S-states, normalized and overplotted for comparison purposes. Black and gray lettering relates to the corresponding curves for each of the three pairs. S_2 is shifted to lower energy relative to S_1 and S_0 is at higher energy relative to S_1; S_2 and S_3 are essentially the same. These comparisons are more easily seen in the XES difference spectra (right frame).

by mixing with ligand orbitals that may be perturbed by small changes in geometry of the cluster that occur between S_2 and S_3. The relative independence of XES to coordination environment has been verified by studies using model Mn complexes with different ligands and nuclearities (Visser et al. 2001; Pizarro et al. 2004). At the same time it is worth noting that this need not be an all-or-none situation. If the Mn is not oxidized, presumably some other species (a protein side-chain ligand or bound water) is oxidized. The delocalization of the electronic charge from a Mn atom to the ligand could account for the small residual changes seen in the X-ray energies. Such shifts in electronic charge are reflected in the degree of covalency of the bonds (Glaser et al. 2000).

A still smaller influence specific to ligand atoms is seen in transitions involving metal 3d orbitals. Transitions involving these orbitals give rise to the pre-edge features and are involved in resonant inelastic X-ray scattering (RIXS) measurements (Glatzel et al. 2004). RIXS data yield two-dimensional plots (Figures 5a and b) that can be interpreted along the incident (absorption) energy or the energy transfer axis. The second dimension separates the pre-edge (predominantly 1s $\rightarrow$ 3d transitions) from the main K-edge. Analysis of RIXS spectra for the S_1- and S_2-states, for example, indicates that the electron involved in this step is transferred from a strongly delocalized orbital.

Comparison of the XANES, XES and RIXS data from Mn model compounds with those from PS II samples provides us with a method for assigning the formal oxidation states of the Mn atoms in the various S-states (Yachandra 2002). Our studies support the assignment of formal oxidation states (III_2,IV_2) and (III,IV_3) in the S_1 and S_2 states, respectively. The S_2 to S_3 transition, as described above, is not a Mn-centered oxidation. The S_0 to S_1 transition can be either a Mn(II) to Mn(III) or a Mn(III) to Mn(IV) oxidation; hence, the Mn in the S_0 state can be in either the oxidation states (II,III,IV_2) or (III_3, IV).

Structure and orientation of the Mn_4Ca cluster

On the basis of Mn EXAFS measurements on a variety of model complexes, it was proposed that the 2.7 Å Mn–Mn vector (peak II) is associated with di-μ-oxo bridged binuclear Mn. Assuming that each Mn atom is 5- or, more likely, 6-coor-

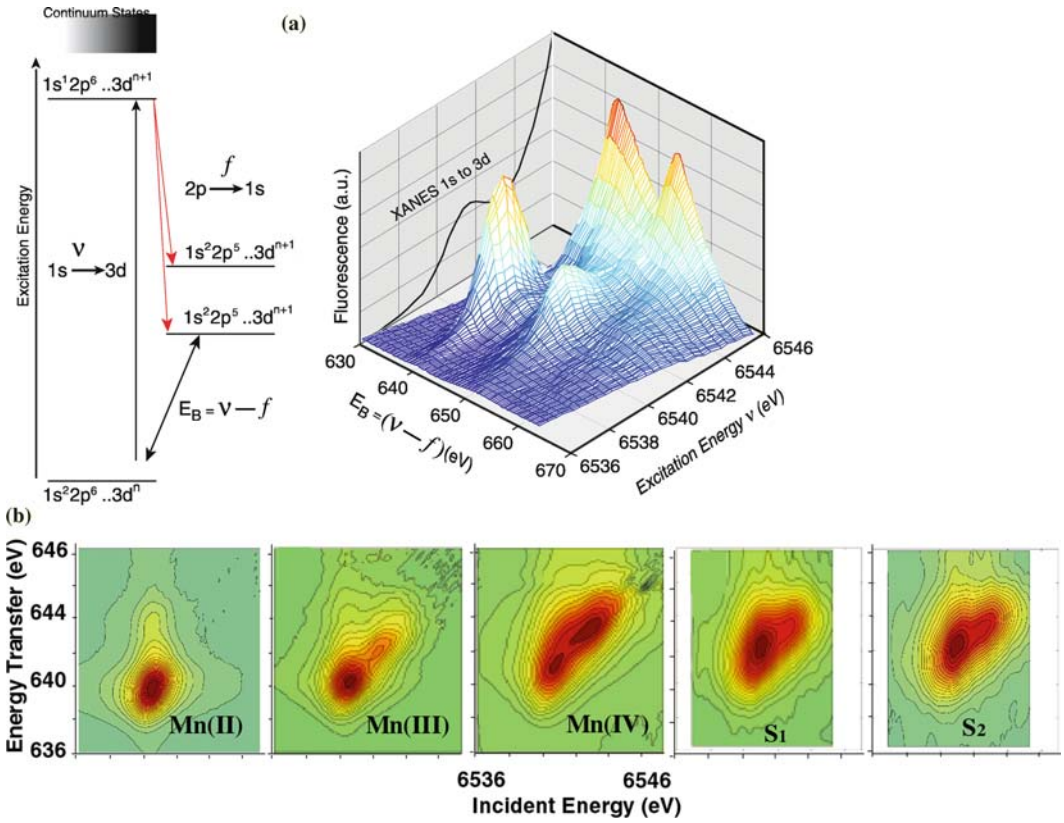

Figure 5. (a) A two-dimensional plot showing the resonant inelastic X-ray spectrum from a Mn(II)acetylacetonate complex. *X*-axis is the excitation energy across the 1s–3d energy range of the spectrum. The 1s–3d K-edge spectrum is plotted in the back of the 2-dimensional spectrum for reference. *Y*-axis is the difference between the excitation and emission energy. The deconvolution of the 1s–3d spectrum as shown in the 2D plot is significantly better than one can obtain from a simple K-edge spectrum. An integration of the 2D plot parallel to the *y*-axis yields L-edge like spectra, the more intense feature at 640 eV corresponds to transitions to $J = 3/2$ like states (L_3 edges) and transitions to 655 eV correspond to $J = 1/2$ final states (L_2 edges). Integrations parallel to the energy transfer axis sort the spectrum according to the final state. (b) Contour plots of the $1s2p_{3/2}$ RIXS planes for three molecular complexes $Mn^{II}(acac)_2(H_2O)_2$, $Mn^{III}(acac)_3$, and $Mn^{IV}(sal)_2(bipy)$ and PS II in the S_1- and S_2-state. One axis is the excitation energy and the other is the energy transfer axis. The L-edge like spectra are along the energy transfer axis and the 1s to 3d transition is along the excitation energy. The assignment of $Mn(III_2, IV_2)$ for the S_1 state is apparent in these spectra (Glatzel et al. 2004).

dinated, the two components of Peak I are from Mn–O bonds in the bridges at 1.8 Å and Mn–O,N terminal ligand bonds at 2.0 Å. Simulations of the spectra indicated that there were at least two (Guiles et al. 1990a) and possibly three (Penner-Hahn et al. 1990; Penner-Hahn 1998) of the Mn–Mn vectors present. Although there was no difference in EXAFS between the S_1 and S_2 states that was distinguishable at the time, a decrease of the Peak II amplitude was noted for the S_3 state (Yachandra et al. 1989), and subsequent studies of the S_3-state EXAFS showed resolution of two distance components in this peak (Guiles et al. 1990a; Liang et al. 2000). In the earlier studies, the only reliable EXAFS of a sample thought to resemble the S_0-state was achieved by treating PS II in the S_1-state with low concentrations of certain reducing agents like NH_2 OH and giving a short illumination (Yachandra et al. 1986a, 1989; Guiles et al. 1990b). As already noted, these samples exhibited a lower Mn K-edge energy indicating a lower average oxidation state of Mn relative to the S_1-state. Because it was not produced by normal progress forward through the Kok cycle, it was designated the S_0*-state. Careful analysis of the EXAFS of the S_0*-state showed evidence of heterogeneity in peak II for this preparation, as well as for the S_3-state (Guiles et al. 1990b). In summary, the EXAFS measurements demonstrated that the structure of the Mn_4 cluster is very similar in all four S-states that have been studied. The changes in

Mn–Mn distances seen in S_0* and S_3 relative to S_1 and S_2 are less than 0.2 Å.

A popular early topological model for the Mn cluster was the dimer-of-dimers model. This consisted of two separate di-μ-oxo bridged binuclear Mn pairs connected by a mono-oxo link. In a recent study, evidence was found for the presence of three Mn–Mn vectors in peak II (Robblee et al. 2002). Several models incorporating a 3 + 1 arrangement of Mn atoms in the cluster had been put forward previously (DeRose et al. 1994). All of these were shown to be present in manganese oxide minerals that may have provided materials for the natural incorporation of such a cluster at the time of the first appearance of oxygenic photosynthesis perhaps 3.5 Ga ago (Sauer and Yachandra 2002). Further support for a 3 + 1 structure (Figure 6) comes from magnetic resonance experiments (Peloquin et al. 2000) and from theoretical studies using density functionals (Siegbahn 2000; Lundberg and Siegbahn 2004).

Calcium ion is essential for O_2 evolution by PS II. Depletion of Ca^{2+} from the samples by various treatments leads to loss of activity, which can be restored by reconstitution with Ca^{2+} or, to a lesser extent, with Sr^{2+}. Other cations are much less effective (Debus 1992). Yachandra et al. (1993) reported that reconstitution with Sr^{2+} resulted in an increase in Peak III amplitude in Mn EXAFS relative to that of Ca-reconstituted samples. This was considered to be an indication of a contribution to Peak III from a Mn–Ca interaction, which became enhanced when Ca was replaced by the heavier Sr atom. This result was confirmed in a subsequent study by Latimer et al. (1995), but was disputed in a report on studies of a PS II preparation from which two extrinsic proteins associated with water oxidation, the 24 kDa (PsbP) and 17 kDa (PsbQ) proteins, were removed (Riggs-Gelasco et al. 1996). To resolve the question of whether a Mn–Ca(Sr) interaction contributes to Peak III, an experiment of the reverse type was carried out. X-ray radiation at the K-edge of Sr was used to examine a Sr-reconstituted PS II preparation, and a strong peak at 3.5 Å was seen in the Sr EXAFS (Cinco et al. 1998). Furthermore, this peak disappeared when the Mn was removed from the membranes by treatment with higher concentrations of NH_2OH. Subsequent studies using Ca EXAFS confirmed these results (Figure 7) and verified that the cluster contains one or two Mn–Ca vectors at 3.4 Å (Cinco et al. 2002).

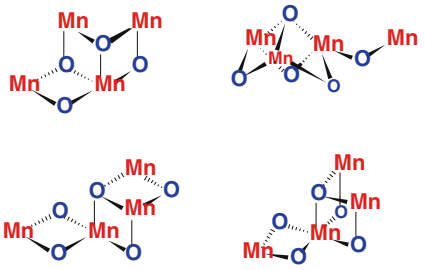

Figure 6. Cluster arrangements of 4 Mn atoms bridged by O atoms and exhibiting three di-μ-oxo bridged Mn–Mn pairs.

Oriented samples of PS II membranes exhibit polarization-dependent absorption (dichroism) in their X-ray spectra (George et al. 1989). Dichroism in the K-edge XANES region reflects transitions to different unoccupied metal orbitals and, in principle, provides information about the identity and orientation of these orbitals. The XANES structure in the so-called pre-edge region involving 1s to 3d transitions has been interpreted using a quantum mechanical approach for several transition metal complexes of known structure (Glaser et al. 2000), but the complicated contributions superimposed from four differently situated Mn in the unknown structure of the cluster in PS II presents a barrier to interpretation.

Dichroism in the EXAFS is more tractable despite limitations in the complete ordering of

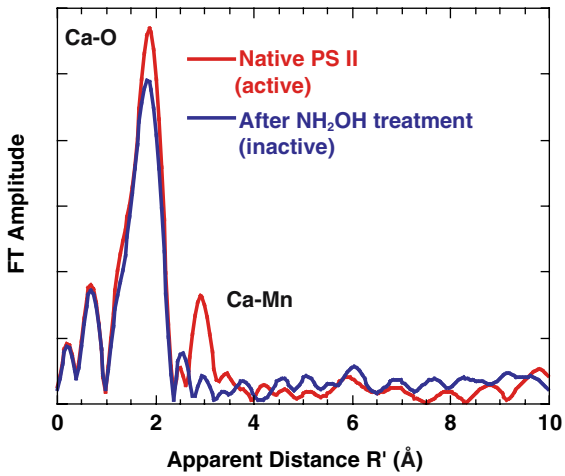

Figure 7. Ca-EXAFS of Photosystem II membranes in the S_1-state. Sample containing approx. 2 Ca per PS II (solid curve). Sample treated with NH_2OH to remove Mn (broken curve). The disappearance of the peak labeled II in the EXAFS of the NH_2OH-treated sample indicates the presence of a Mn–Ca interaction at 3.3 Å.

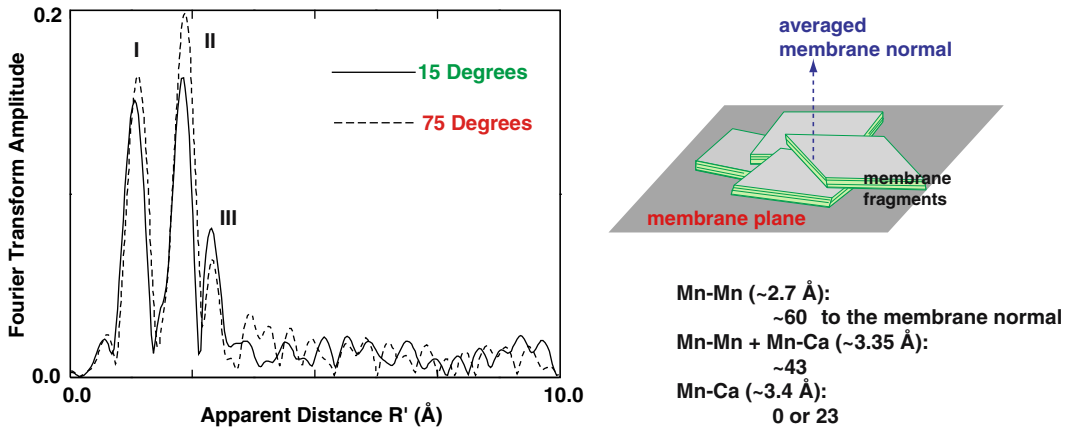

Figure 8. Mn-EXAFS dichroism of PS II membranes in the S_1-state oriented by layering, as illustrated at the right. Samples oriented with the membrane normals at 15° (solid curve) and 75° (broken curve) to the electric vector of the incident X-ray beam. Peaks labeled I, II and III correspond to those described in the caption to Figure 3. The presence of dichroism is indicated by the different relative peak heights for measurements at the different angles.

membrane preparations that lead to a phenomenon known as mosaic spread. This results in a distribution in the angles, typically ±15 to ±25°, between the membrane normals of individual thylakoid membranes and the supporting surface. The consequence of this imperfect ordering is an increased uncertainty of the true angle between a binuclear atom vector, as seen in the EXAFS, and the membrane normal. Nevertheless, important geometric insights can be derived from these measurements. Although all three characterized peaks in the Mn EXAFS exhibit dichroism (Figure 8), there are too many contributions to Peak I from O- and N-atom ligands to permit meaningful interpretation. Peak II shows pronounced dichroism resulting from the Mn–Mn vectors, which exhibit an average inclination of 60° (±7° and ±4°) from the membrane normal in the

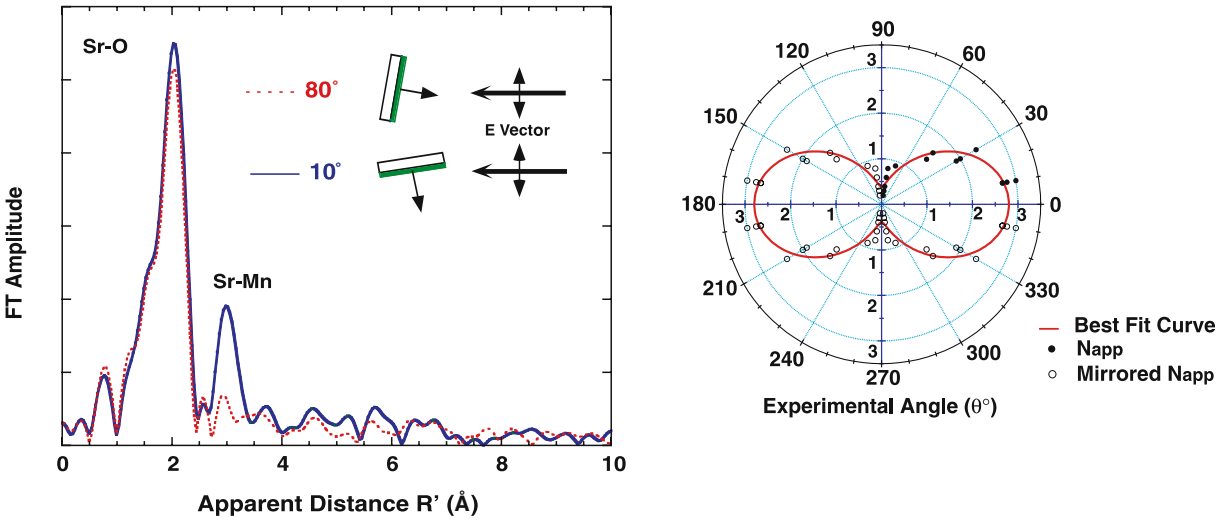

Figure 9. Sr-EXAFS dichroism of PS II membranes from which Ca has been extracted and reconstituted with Sr. Oriented membranes and dichroism measured as described in the caption to Figure 8. Spectra for samples oriented at 10 and 80° are shown (left frame). The polar plot (right frame) summarizes the normalized intensity of peak II for samples measured at a variety of angles. (Measurements shown in the first quadrant are repeated in the other three quadrants to show the expected symmetry. The solid curve is fit to the data.) Results indicate that the Sr–Mn vector(s) at 3.5 Å are oriented close to the membrane normal.

S_1- and S_2-states, respectively (Mukerji et al. 1994). The Mn–Mn and Mn–Ca vectors contributing to Peak III exhibit an average inclination of 43° (±11° and ±10°) from the membrane normal. Binding of NH_3, an analog of substrate water, to PS II inhibits O_2 evolution. Illumination of NH_3-treated PS II particles produces a preparation that shows a splitting of Peak II that reflects an increase of one of the Mn–Mn vectors from 2.72 to 2.87 Å (Dau et al. 1995). Furthermore, analysis of the dichroism of oriented membranes from the S_2-state of the NH_3-treated PS II shows that the resolved vectors are at 55° ± 4° and 67° ± 3°, respectively, to the membrane normal. The fact that these numbers average to nearly 60° is suggestive that there are no large structural changes associated with NH_3 binding. A further analysis of the Peak III dichroism was facilitated by polarized Sr-EXAFS measurements on Sr-substituted PS II (Cinco et al. 2004). The Sr EXAFS of oriented PS II is very strongly dichroic (Figure 9), indicating that the Sr–Mn vector(s) lie at 0° or 23° of the membrane normal. Deconvolution of the Mn EXAFS dichroism of peak III (Figure 8), which contains contributions from both Mn–Mn and Mn–Ca(Sr), is complicated by uncertainty as to the relative contributions of Mn or Ca(Sr) to the scattering. Three model clusters that incorporate Mn and Ca and are consistent with the polarized EXAFS of PS II are shown in Figure 10.

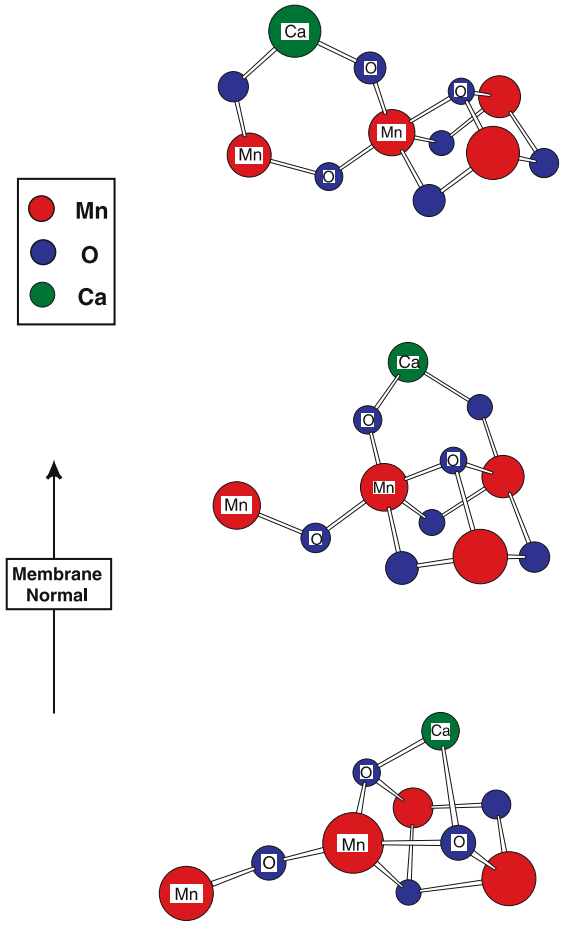

Figure 10. Cluster arrangements of 4 Mn and 1 Ca bridged by O atoms and consistent with the Mn- and Sr-EXAFS dichroism.

New directions

Several unresolved problems are being addressed through new directions that are being pursued in different laboratories.

An alternative application of polarized X-ray spectroscopy involves the use of oriented single crystals. In collaboration with Drs Athina Zouni, Jan Kern and Johannes Messinger, we are pursuing such studies using PS II single crystals. An example of polarized X-ray spectra of a Mn model compound is shown in Figure 11 (Yano et al. 2004). Crystals of PS II from thermophilic cyanobacteria and X-ray diffraction analysis have been reported from groups in Berlin (Zouni et al. 2001), in Japan (Kamiya and Shen 2003) and in London (Ferreira et al. 2004). Although the resolution reported to date is limited to 3.2 Å (Biesiadka et al. 2004) which is far from atomic resolution, nevertheless the crystal symmetry, the general arrangement of the protein components, the disposition of pigment molecules and the location of the Mn_4Ca cluster have been identified. PS II as isolated from the cyanobacteria consists of dimers, and the crystals contain four dimers per unit cell for a total of eight Mn clusters altogether. The four dimers in the orthorhombic crystals are symmetrically equivalent; however, the two oxygen-evolving centers in each dimer are related by a non-crystallographic C_2 rotation. This provides a complication in the interpretation of polarized X-ray spectra. Both XANES and EXAFS of PS II crystals exhibit pronounced dichroism, as the orientation of the crystallographic axes is changed relative to the direction of the *E*-vector of the polarized X-ray beam. A test of the consistency of the dichroism components is obtained by averag-

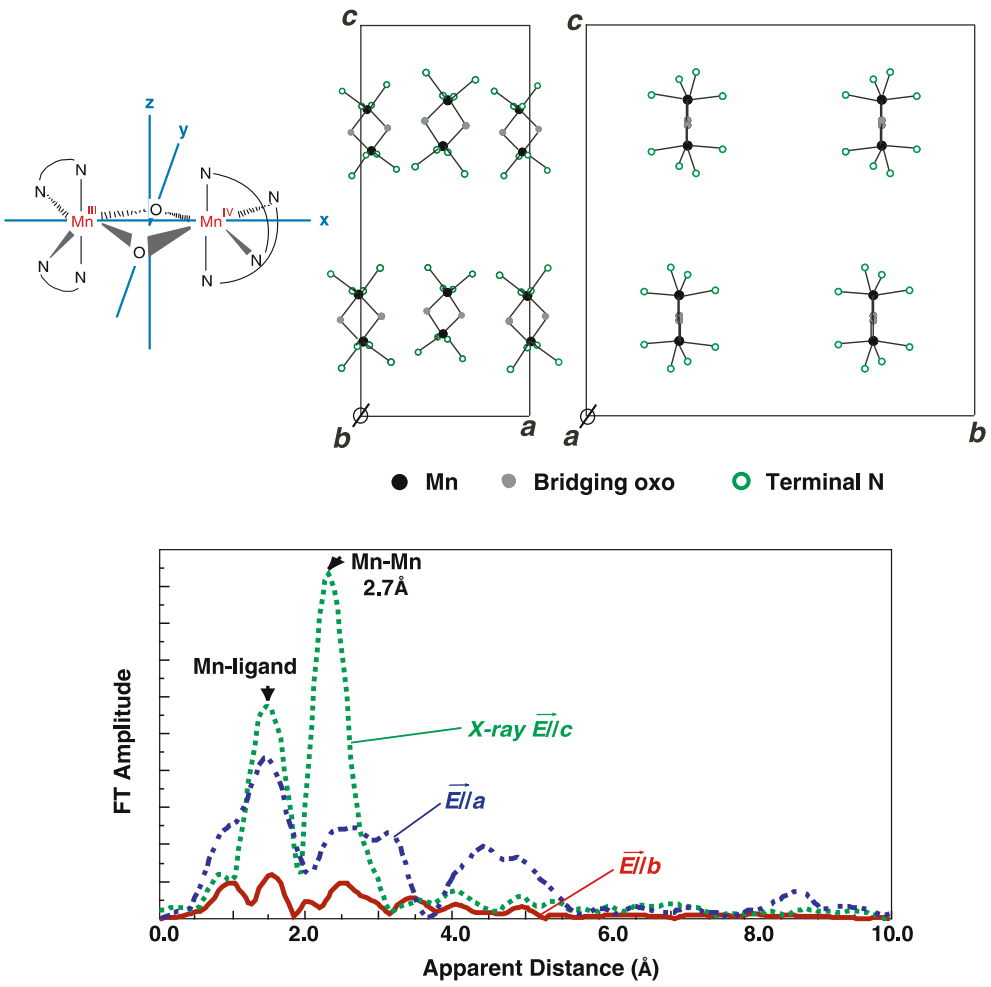

Figure 11. Single-crystal Mn-EXAFS of $[Mn_2(III,IV)O_2(phen)_4](PF_6)_3CH_3CN$, where phen = 1,10-phenanthroline. A schematic of the molecular structure is shown together with projections onto the ac- and bc-planes of these orthorhombic crystals (upper frame). Mn EXAFS measured with the *a*- (dash-dot curve), *b*- (solid curve) and *c*-axes (dotted curve) aligned with the *E*-vector of the incident X-ray beam are shown (lower frame). The strong polarization of the 2.7 Å Mn–Mn peak along the *c*-axis is consistent with the crystal structure.

ing overall orientations, and comparing with the XAS of an isotropic sample, where it is seen that the observed and simulated spectra are essentially indistinguishable (J. Yano et al., in preparation). Analysis of the polarized EXAFS from single PS II crystals is proceeding with regard to the 3 + 1 cluster models and the information already obtained from the dichroism studies on oriented membranes.

An extended range of EXAFS data can be collected using a high resolution crystal monochromator that removes the interference arising from Fe present in the PS II samples (J. Yano et al., in preparation). This permits a better resolution of composite peaks where two or more different distances contribute. Better resolution is particularly beneficial for analysis of single crystals of PS II using polarized radiation, because the different contributing vectors typically project differently onto the crystal axes. It will also be useful for doing quantitative deconvolution of these composite peaks to determine the exact number of contributing vectors.

Time-dependent XAS with sub-μs time resolution opens the possibility of identifying and characterizing intermediates in the individual S-state transitions that have not yet been documented (Haumann et al. 2002). Of particular interest is the

series of events on the ms time scale that accompany the formation of dioxygen during the S_4 to S_0 transition.

Summary

X-ray spectroscopy of the Mn_4Ca cluster of the water-oxidation complex of PS II provides information about the oxidation states and cluster geometry in samples that are active in O_2 evolution. Advances in the Kok-cycle from S_0 to S_1 and from S_1 to S_2 show clear evidence of Mn oxidation, whereas the advance from S_2 to S_3 does not. These conclusions, originally based on XANES measurements, have been strengthened by the results of XES studies. The application of EXAFS analysis has established the importance of di-μ-oxo bridged pairs of Mn atoms in the cluster. Quantitative studies support the presence of three such Mn–Mn vectors at about 2.7 Å distance in the S_1- and S_2-states, that becomes resolved into multiple distances in the S_3- and S_0-states. Changes in geometry are relatively small (<0.2 Å) among all four stabilized S-states, however. A composite peak at 3.3–3.4 Å contains contributions from both Mn–Mn and Mn–Ca vectors. Dichroism measurements on oriented membranes containing PS II place limitations on the geometry of the cluster relative to the membrane normal. Models of the cluster involving a 3 + 1 arrangement of four Mn atoms and with bridging to Ca are presented that are consistent with the polarized EXAFS.

Acknowledgements

The research was supported by the NIH (GM 55302), and the DOE, Director, Office of Science, Office of Basic Energy Sciences, Chemical Sciences, Geosciences, and Biosciences Division, under Contract DE-AC03-76SF00098. Synchrotron radiation facilities were provided by SSRL, APS and ALS, which are supported by DOE, Office of Basic Energy Sciences. The SSRL Biotechnology Program is supported by NIH, National Center of Research Resources, Biomedical Technology Program, and by DOE, Office of Health and Environmental Research. BioCAT at the APS is a NIH-supported Research Center RR-08630.

References

Bergmann U, Grush MM, Horne CR, DeMarois P, Penner-Hahn JE, Yocum CF, Wright DW, Dubé CE, Armstrong WH, Christou G, Eppley HJ and Cramer SP (1998) Characterization of the Mn oxidation states in Photosystem II by Kβ X-ray fluorescence spectroscopy. J Phys Chem B 102: 8350–8352

Biesiadka J, Loll B, Kern J, Irrgang K-D and Zouni A (2004) Crystal structure of cyanobacterial Photosystem II at 3.2 Å resolution: A closer look at the Mn-Cluster. Phys Chem Chem Phys 6: 4733–4736

Blankenship RE (2002) Molecular Mechanisms of Photosynthesis, Blackwell, Oxford

Blankenship RE Madigan MT Bauer CE (eds) (1995) Anoxygenic Photosynthetic Bacteria, Kluwer Academic Publishers, Dordrecht, The Netherlands

Britt RD, Campbell KA, Peloquin JM, Gilchrist ML, Aznar CP, Dicus MM, Robblee J and Messinger J (2004) Recent pulsed EPR studies of the Photosystem II oxygen-evolving complex: implications as to water oxidation mechanisms. Biochim Biophys Acta 1655: 158–171

Cinco RM, Robblee JH, Rompel A, Fernandez C, Yachandra VK, Sauer K and Klein MP (1998) Strontium EXAFS reveals the proximity of calcium to the manganese cluster of oxygen-evolving Photosystem II. J Phys Chem B 102: 8248–8256

Cinco RM, McFarlane Holman KL, Robblee JH, Yano J, Pizarro SA, Bellacchio E, Sauer K and Yachandra VK (2002) Calcium EXAFS establishes the Mn–Ca cluster in the oxygen-evolving complex of Photosystem II. Biochemistry 41: 12928–12933

Cinco RM, Robblee JH, Messinger J, Fernandez C, McFarlane Holman KL, Sauer K and Yachandra VK (2004) Orientation of calcium in the Mn_4Ca cluster of the oxygen-evolving complex determined using polarized strontium EXAFS of Photosystem II membranes. Biochemistry 43: 13271–13282

Dau H, Andrews JC, Roelofs TA, Latimer MJ, Liang W, Yachandra VK, Sauer K and Klein MP (1995) Structural consequences of ammonia binding to the manganese center of the photosynthetic oxygen-evolving complex: an X-ray absorption spectroscopy study of isotropic and oriented Photosystem II particles. Biochemistry 34: 5274–5287

Debus RJ (1992) The manganese and calcium ions of photosynthetic oxygen evolution. Biochim Biophys Acta 1102: 269–352

Debus RJ (2001) Amino acid residues that modulate the properties of tyrosine Y_Z and the manganese cluster in the water oxidizing complex of Photosystem II. Biochim Biophys Acta 1503: 164–186

DeRose VJ, Mukerji I, Latimer MJ, Yachandra VK, Sauer K and Klein MP (1994) Comparison of the manganese oxygen-evolving complex in Photosystem II of spinach and *Synechococcus* sp. with multinuclear manganese model compounds by X-ray absorption spectroscopy. J Am Chem Soc 116: 5239–5249

Ferreira KN, Iverson TM, Maghlaoui K, Barber J and Iwata S (2004) Architecture of the photosynthetic oxygen-evolving center. Science 303: 1831–1838

George GN, Prince RC and Cramer SP (1989) The manganese site of the photosynthetic water-splitting enzyme. Science 243: 789–791

Glaser T, Hedman B, Hodgson KO and Solomon EI (2000) Ligand K-edge absorption spectroscopy: a direct probe of ligand – metal covalency. Acc Chem Res 33: 859–868

Glatzel P, Bergmann U, Yano J, Visser H, Robblee JH, Gu W, de Groot FMF, Christou G, Pecoraro VL, Cramer SP and Yachandra VK (2004) The electronic structure of Mn in oxides, coordination complexes, and the oxygen-evolving complex of Photosystem II studied by resonant inelastic X-ray scattering. J Am Chem Soc 126: 9946–9959

Goodin DB, Yachandra VK, Britt RD, Sauer K and Klein MP (1984) The state of manganese in the photosynthetic apparatus. 3. Light-induced changes in X-ray absorption (K-edge) energies of manganese in photosynthetic membranes. Biochim Biophys Acta 767: 209–216

Guiles RD, Zimmermann J-L, McDermott AE, Yachandra VK, Cole JL, Dexheimer SL, Britt RD, Wieghardt K, Bossek U, Sauer K and Klein MP (1990a) The S_3 state of Photosystem II: differences between the structure of the manganese complex in the S_2 and S_3 states determined by X-ray absorption spectroscopy. Biochemistry 29: 471–485

Guiles RD, Yachandra VK, McDermott AE, Cole JL, Dexheimer SL, Britt RD, Sauer K and Klein MP (1990b) The S_0 state of Photosystem II induced by hydroxylamine: Differences between the structure of the manganese complex in the S_0 and S_1 states determined by X-ray absorption spectroscopy. Biochemistry 29: 486–496

Haumann M, Grabolle M, Neisius T and Dau H (2002) The first room-temperature X-ray absorption spectra of higher oxidation states of the tetra-manganese complex of Photosystem II. FEBS Lett 512: 116–120

Iuzzolino L, Dittmer J, Dörner W, Meyer-Klaucke W and Dau H (1998) X-ray absorption spectroscopy on layered Photosystem II membrane particles suggests manganese-centered oxidation of the oxygen-evolving complex for the S_0–S_1, S_1–S_2, and S_2 –S_3 transitions of the water oxidation cycle. Biochemistry 37: 17112–17119

Jaklevic J, Kirby JA, Klein MP, Robertson AS, Brown GS and Eisenberger P (1977) Fluorescence detection of EXAFS: sensitivity enhancement for dilute species and thin films. Solid State Commun 23: 679–682

Kamiya N and Shen J-R (2003) Crystal structure of oxygen-evolving Photosystem II from *Thermosynechococcus vulcanus* at 3.7-Å resolution. Proc Natl Acad Sci USA 100: 98–103

Kirby JA, Robertson AS, Smith JP, Thompson AC, Cooper SR and Klein MP (1981a) State of manganese in the photosynthetic apparatus. 1. Extended X-ray absorption fine structure studies on chloroplasts and di-μ-oxo bridged dimanganese model compounds. J Am Chem Soc 103: 5529–5537

Kirby JA, Goodin DB, Wydrzynski T, Robertson AS and Klein MP (1981b) State of manganese in the photosynthetic apparatus. 2. X-ray absorption edge studies on manganese in photosynthetic membranes. J Am Chem Soc 103: 5537–5542

Latimer MJ, DeRose VJ, Mukerji I, Yachandra VK, Sauer K and Klein MP (1995) Evidence for the proximity of calcium to the manganese cluster of Photosystem II: determination by X-ray absorption spectroscopy. Biochemistry 34: 10898–10909

Liang W, Roelofs TA, Cinco RM, Rompel A, Latimer MJ, Yu WO, Sauer K, Klein MP and Yachandra VK (2000) Structural change of the Mn cluster during the $S_2 \rightarrow S_3$ state transition of the oxygen-evolving complex of Photosystem II. Does it reflect the onset of water/substrate oxidation? Determination by Mn X-ray absorption spectroscopy. J Am Chem Soc 122: 3399–3412

Lundberg M and Siegbahn PEM (2004) Theoretical investigations of structure and mechanism of the oxygen-evolving complex in PSII. Phys Chem Chem Phys 6: 4772–4780

Messinger J, Robblee JH, Bergmann U, Fernandez C, Glatzel P, Visser H, Cinco RM, McFarlane KL, Bellacchio E, Pizarro SA, Cramer SP, Sauer K, Klein MP and Yachandra VK (2001) Absence of Mn-centered oxidation in the $S_2 \rightarrow S_3$ transition: implications for the mechanism of photosynthetic water oxidation. J Am Chem Soc 123: 7804–7820

Mukerji I, Andrews JC, DeRose VJ, Latimer MJ, Yachandra VK, Sauer K and Klein MP (1994) Orientation of the oxygen-evolving manganese complex in a Photosystem II membrane preparation: an X-ray absorption spectroscopy study. Biochemistry 33: 9712–9721

Olesen K and Andréasson LE (2003) The function of the chloride ion in photosynthetic oxygen evolution. Biochemistry 42: 2025–2035

Ono T-A, Noguchi T, Inoue Y, Kusunoki M, Matsushita T and Oyanagi H (1992) X-ray detection of the period-four cycling of the manganese cluster in photosynthetic water oxidizing enzyme. Science 258: 1335–1337

Ono T-A, Noguchi T, Inoue Y, Kusunoki M, Yamaguchi H and Oyanagi H (1995) XANES spectroscopy for monitoring intermediate reaction states of Cl-depleted Mn cluster in photosynthetic water oxidation enzyme. J Am Chem Soc 117: 6386–6387

Peloquin JM, Campbell KA, Randall DW, Evanchik MA, Pecoraro VL, Armstrong WH and Britt RD (2000) ^{55}Mn ENDOR of the S_2-state multiline EPR signal of Photosystem II: implications on the structure of the tetranuclear Mn cluster. J Am Chem Soc 122: 10926–10942

Penner-Hahn JE (1998) Structural characterization of the Mn site in the photosynthetic oxygen-evolving complex. Structure Bonding 90: 1–35

Pizarro S, Glatzel P, Visser H, Robblee JH, Christou G, Bergmann U and Yachandra VK (2004) Mn oxidation states in tri- and tetra-nuclear Mn compounds structurally relevant to Photosystem II: Mn K-edge X-ray absorption and Kβ X-ray emission spectroscopy studies. Phys Chem Phys 20: 4864–4870

Powers L (1982) X-ray absorption spectroscopy. Application to biological molecules. Biochim Biophys Acta 683: 1–38

Renger G (2001) Photosynthetic water oxidation to molecular oxygen: apparatus and mechanism. Biochim Biophys Acta 1503: 210–228

Riggs-Gelasco PJ, Mei R, Ghanotakis DF, Yocum CF and Penner-Hahn JE (1996) X-ray absorption spectroscopy of calcium-substituted derivatives of the oxygen-evolving complex of Photosystem II. J Am Chem Soc 118: 2400–2410

Robblee JH, Messinger J, Cinco RM, McFarlane KL, Fernandez C, Pizarro SA, Sauer K and Yachandra VK (2002) The Mn cluster in the S_0 state of the oxygen evolving complex of Photosystem II studied by EXAFS spectroscopy: are there three di-μ-oxo bridged Mn_2 moieties in the tetrameric Mn complex,. J Am Chem Soc 124: 7459–7471

Roelofs TA, Liang W, Latimer MJ, Cinco RM, Rompel A, Andrews JA, Sauer K, Yachandra VK and Klein MP (1996) Oxidation states of the manganese cluster during the flash-induced S-state cycle of the photosynthetic oxygen-evolving complex. Proc Natl Acad Sci USA 93: 3335–3340

Sauer K and Yachandra VK (2002) A possible evolutionary origin for the Mn_4 cluster of the photosynthetic water oxidation complex from natural MnO_2 precipitates in the early ocean. Proc Natl Acad Sci USA 99: 8631–8636

Schopf JW (1999) The Cradle of Life, Princeton University Press, Princeton, NJ

Siegbahn PEM (2000) Theoretical models for the oxygen radical mechanism of water oxidation and of the water oxidizing complex of Photosystem II. Inorg Chem 39: 2923–2935

Visser H, Anxolabéhère-Mallart E, Bergmann U, Glatzel P, Robblee JH, Cramer SP, Girerd J-J, Sauer K, Klein MP and Yachandra VK (2001) Mn K-edge XANES and Kβ XES studies of two Mn–oxo binuclear complexes: investigation of three different oxidation states relevant to the oxygen-evolving complex of Photosystem II. J Am Chem Soc 123: 7031–7039

Yachandra VK (1995) X-ray absorption spectroscopy and applications in structural biology. Meth Enzymol 246: 638–675

Yachandra VK (2002) Structure of the manganese complex in Photosystem II: insights from X-ray spectroscopy. Phil Trans R Soc Lond B 357: 1347–1358

Yachandra VK, Guiles RD, McDermott A, Britt RD, Cole J, Dexheimer SL, Sauer K and Klein MP (1986a) The state of manganese in the photosynthetic apparatus determined by X-ray absorption spectroscopy. J Phys C 8: 1121–1128

Yachandra VK, Guiles RD, McDermott A, Britt RD, Dexheimer SL, Sauer K and Klein MP (1986b) The state of manganese in the photosynthetic apparatus. 4. Structure of the manganese complex in Photosystem II studied using EXAFS spectroscopy. The S_1 state of the O_2-evolving Photosystem II complex from spinach. Biochim Biophys Acta 850: 324–332

Yachandra VK, DeRose VJ, Latimer MJ, Mukerji I, Sauer K and Klein MP (1993) Where plants make oxygen: a structural model for the photosynthetic oxygen-evolving manganese cluster. Science 260: 675–679

Yachandra VK, Sauer K and Klein MP (1996) Manganese cluster in photosynthesis: where plants oxidize water to dioxygen. Chem Rev 96: 2927–2950

Yano J, Sauer K, Girerd J-J and Yachandra VK (2004) Single crystal X- and Q-band EPR spectroscopy of a binuclear Mn_2 (III,IV) complex relevant to the oxygen-evolving complex of Photosystem II. J Am Chem Soc 126: 7486–7495

Zouni A, Witt H-T, Kern J, Fromme P, Krauss N, Saenger W and Orth P (2001) Crystal structure of Photosystem II from *Synechococcus elongatus* at 3.8 Å resolution. Nature 409: 739–743